




Cite this: DOI: 10.1039/c8nr08727j

## In-place bonded semiconductor membranes as compliant substrates for III–V compound devices†

Ailton J. Garcia Jr., <sup>a</sup> Leonarde N. Rodrigues,<sup>a,b</sup> Saimon Filipe Covre da Silva,<sup>‡,a,b</sup> Sergio L. Morelhão,<sup>c</sup> Odilon D. D. Couto Jr.,<sup>d</sup> Fernando Iikawa<sup>d</sup> and Christoph Deneke<sup>\*a,d</sup>

Overcoming the critical thickness limit in pseudomorphic growth of lattice mismatched heterostructures is a fundamental challenge in heteroepitaxy. On-demand transfer of light-emitting structures to arbitrary host substrates is an important technological method for optoelectronic and photonic device implementation. The use of freestanding membranes as compliant substrates is a promising approach to address both issues. In this work, the feasibility of using released GaAs/InGaAs/GaAs membranes as virtual substrates to thin films of InGaAs alloys is investigated as a function of the indium content in the films. Growth of flat epitaxial films is demonstrated with critical thickness beyond typical values observed for growth on bulk substrates. Optically active structures are also grown on these membranes with a strong photoluminescence signal and a clear red shift for an InAlGaAs/InGaAs/InAlGaAs quantum well. The red shift is ascribed to strain reduction in the quantum well due to the use of a completely relaxed membrane as the substrate. Our results demonstrate that such membranes constitute a virtual substrate that allows further heterostructure strain engineering, which is not possible when using other post-growth methods.

Received 29th October 2018,  
Accepted 21st January 2019

DOI: 10.1039/c8nr08727j

rscl.li/nanoscale

## Introduction

Mastering the ability to fabricate freestanding, extremely thin semiconductor layers<sup>1–6</sup> – transferable and integrable into flexible electronics – and using them as virtual substrates can be viewed as a key issue in advancing heteroepitaxial growth towards different classes of nanostructured devices.<sup>7–15</sup> This approach can overcome one of the fundamental challenges in heteroepitaxy: the critical thickness for the pseudomorphic growth of lattice mismatched heterostructures<sup>16,17</sup> (as well as the strain effects due to lattice mismatch). Indeed, for an arbitrary heterostructure, there is a limited choice of substrates to grow strain-free structures as illustrated in Fig. 1(a) for an In<sub>0.10</sub>Ga<sub>0.90</sub>As layer. For such a layer, no common substrate exists that allows strain-free growth. Therefore, all available substrates limit the achievable layer thickness due to defect formation beyond a critical thickness. Furthermore, with a

strain in the heterostructure, its physical properties change, *e.g.* the emission energy of an In<sub>0.10</sub>Ga<sub>0.90</sub>As based quantum well (QW) shifts by the following approximation:  $\Delta E = 5.8 \times \epsilon$  eV (with  $\epsilon$  being a biaxial strain in the structure and  $\Delta E$  the shift in emission energy).<sup>18</sup>

Already in the 1990s, Lo *et al.*<sup>19</sup> pointed out that a thin compliant substrate could be a solution to this problem and first growth studies were carried out.<sup>17,19–21</sup> This approach partly lost attention as it involved freestanding structures, which render device fabrication difficult as the suggested cantilever structures were very fragile. With the advent of semiconductor membranes fabricated by the release and rearrangement of heterostructures,<sup>1–3,5,6,22,23</sup> which are transferable and integrable into a flexible electronic structure,<sup>3,22,24,25</sup> the technique has undergone a renaissance.<sup>9–15</sup> In recent years, semiconductor membranes have been used to manufacture self-ordered Ge islands,<sup>12,13</sup> influence the formation of InAs on freestanding Si membranes,<sup>9</sup> or to investigate the modulation of the surface chemical potential to influence epitaxial growth.<sup>10,11</sup> Thereby, the use of completely relaxed, in-place bonded membranes<sup>23</sup> appears extremely attractive as such structures should be suitable for post-processing of the heterostructures. Furthermore, membranes transferred before overgrowth allow the construction of a growth template on any host substrate.<sup>22,26</sup> Recently, silicon membranes transferred before growth to a new host substrate were successfully used as virtual substrates.<sup>14,15</sup> Similar experiments for III–V semi-

<sup>a</sup>Laboratório Nacional de Nanotecnologia (LNNano), Centro Nacional de Pesquisa em Energia e Materiais (CNPEN), Campinas, SP, Brasil.  
E-mail: cdeneke@ifl.unicamp.br

<sup>b</sup>Departamento de Física, Universidade Federal de Viçosa (UFV), Viçosa, MG, Brasil

<sup>c</sup>Instituto de Física, Universidade de São Paulo (USP), São Paulo, SP, Brasil

<sup>d</sup>Instituto de Física “Gleb Wataghin”, Universidade Estadual de Campinas (Unicamp), Campinas, SP, Brasil

†Electronic supplementary information (ESI) available. See DOI: 10.1039/c8nr08727j

‡Current address: Johann Kepler Universität, Linz, Austria.

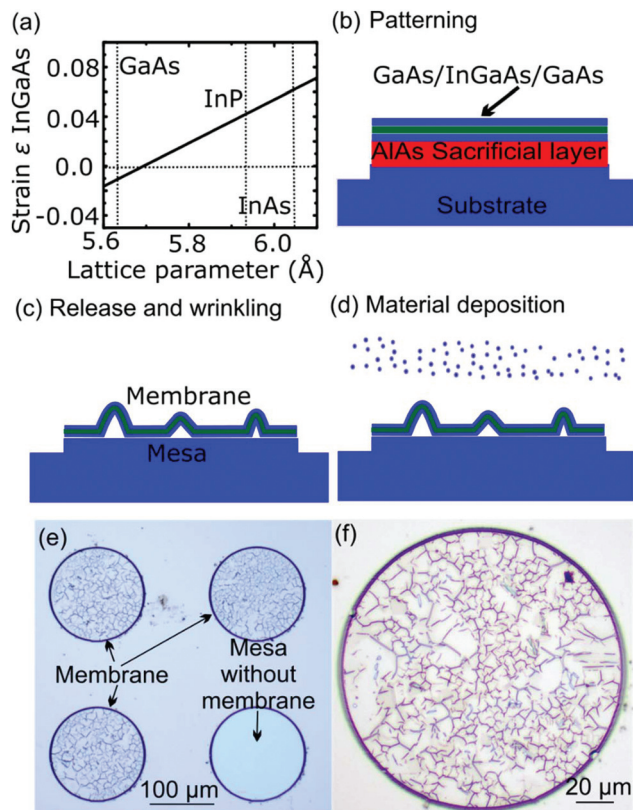


**Fig. 1** (a) Strain of an  $\text{In}_{10}\text{Ga}_{0.9}\text{As}$  layer as a function of the substrate lattice parameter. The lattice parameter of the three most common III–V semiconductor substrates (GaAs, InP, and InAs) is marked. (b)–(d) Fabrication process. (e) Optical microscopy image of processed mesas with released, relaxed, and in-place bonded membranes. In one of them, on the lower right, the released membrane has been detached during lift off and left a bare GaAs (001) substrate serving as a reference position on the sample. (f) Light microscopy image of a single mesa with a released membrane. One can identify larger wrinkled areas and flat areas in between.

conductors are missing, even though this material class is well established for the strain engineering of optical and electrical functional devices.<sup>5,27</sup>

In this work, we investigate the overgrowth behavior on a virtual substrate based on a completely released, wrinkled, and in-place bonded GaAs/InGaAs/GaAs membrane. Overgrown samples are characterized using atomic force microscopy (AFM), scanning electron microscopy (SEM), 3D reciprocal space mapping obtained under grazing incidence X-ray diffraction (XRD) geometry, and micro- and macro-photoluminescence ( $\mu\text{-PL}$ ) measurements. Results from microscopy show a flat  $\text{In}_x\text{Ga}_{1-x}\text{As}$  layer growth up to  $x = 0.4$  on the membrane, whereas layers on the GaAs (001) substrate already show islands and introduce dislocation formation at  $x > 0.3$ . The shift in the critical thickness is supported by the XRD results and associated with the difference in the lattice parameter between the virtual substrate and GaAs. Furthermore, we observe the formation of bubbles on the membrane for higher indium content as well as material migration and accumu-

lation on the top of wrinkles. To demonstrate the ability to grow optically active III–V structures on membranes, we have deposited a nominally unstrained InAlGaAs/InGaAs/InAlGaAs quantum well (QW) on top of a released wrinkled membrane. We observe a 40 meV red shifted PL signal from this QW compared to a reference grown on GaAs (001) wafers, which indicates a strain-free QW on top of the membrane. Together with our demonstrated ability to transfer thin semiconductor membranes before overgrowth to a new host substrate (see the ESI†), this work establishes III–V semiconductor membranes as a compliant substrate for epitaxy, allowing strain engineering of III–V heterostructures for optical and electrical applications.

## Experimental

Molecular beam epitaxy (MBE) was used to grow the initial heterostructure for membrane fabrication as well as to overgrow the membranes. The initial heterostructure is a 5 nm GaAs/10 nm  $\text{In}_{0.2}\text{Ga}_{0.8}\text{As}$ /5 nm GaAs layer stack grown on top of a 20 nm AlAs sacrificial layer and a GaAs (001) substrate in the MBE of the LNNano/CNPEM (Karl Eberl MBE Komponenten). Following a previously used strategy,<sup>10,11</sup> the initial heterostructure was grown on a 2" wafer and removed from the machine afterwards. The heterostructure was patterned using optical lithography and wet chemical etching in a  $\text{H}_3\text{PO}_4 : \text{H}_2\text{O}_2 : \text{H}_2\text{O}$  solution to define mesa of ca. 150  $\mu\text{m}$  diameter. The mesa diameter is large enough to allow epitaxial growth as well as the future manufacturing of devices like micro light-emitting diodes. After the removal of the photoresist and exposure to oxygen plasma for 10 min, in-place bonded, completely relaxed, wrinkled membranes were fabricated by selective removal of the AlAs sacrificial layer by 15 min etching in HF (3%), which is a very reliable process as shown in the past.<sup>14,24,25</sup> Samples were made epi-ready again by a second chemical cleaning, a 3 min HCl dip, and reintroduced into the MBE.<sup>10,11</sup> Atomic hydrogen cleaning was carried out to remove the native surface oxide and further clean the samples. In a systematic study, 10 nm thick InGaAs layers with different indium concentrations were deposited directly on the cleaned samples (containing now membranes on the top of each mesa) at a nominal substrate temperature of 430  $^\circ\text{C}$  to prevent damaging the membranes. The indium concentrations deposited were 5%, 10% (nominally unstrained towards the membrane), 20%, 30%, 40%, 50%, and 100%. Growth was monitored by reflective high-electron diffraction (RHEED).

For the optically active structure, we grew a QW consisting of a 10 nm  $\text{In}_{0.10}\text{Al}_{0.20}\text{Ga}_{0.70}\text{As}$ /5 nm  $\text{In}_{0.10}\text{Ga}_{0.90}\text{As}$ /10 nm  $\text{In}_{0.10}\text{Al}_{0.20}\text{Ga}_{0.70}\text{As}$  active structure followed by a 5 nm  $\text{In}_{0.10}\text{Ga}_{0.90}\text{As}$  capping layer. The structure was fabricated on both a membrane (with a 10 nm  $\text{In}_{0.10}\text{Ga}_{0.90}\text{As}$  buffer layer) and a GaAs (001) wafer with a 300 nm GaAs buffer layer (to be used as a reference). Growing the InGaAs and InAlGaAs alloys requires adequate ratios of the In–Al–Ga flux. As the MBE is equipped only with one In and Ga cell, we had to interrupt the growth before and after the  $\text{In}_{0.10}\text{Ga}_{0.90}\text{As}$  to adjust the growth

rates. The quaternary alloy has a lattice parameter very close to the ternary  $\text{In}_{0.10}\text{Ga}_{0.90}\text{As}$ .

Scanning electron microscopy (SEM) was carried out in the electron microscopy facilities of the LNNano/CNPEM using a FIE Inspec F50 instrument operating the field emission gun at 20 keV. Samples were tilted to  $55^\circ$  to enhance the contrast and images were taken using the secondary electron detector.

Atomic force microscopy was conducted in the LNNano/CNPEM surface science laboratory using a Park NX 10 or an Analysis NanoIR2 instrument. Both instruments were operated in tapping (or non-contact) mode with standard AFM cantilevers with a resonance frequency close to 300 kHz. Besides AFM topography images, AFM phase images were also obtained.

X-ray diffraction (XRD) was carried out at the XRD2 beamline of the Brazilian Synchrotron Light Laboratory (LNLS/CNPEM). The beam was vertically focused with a bent Rh-coated mirror, which filtered higher-order harmonics. The beam energy was tuned to 8 keV using a double-bounce Si(111) monochromator placed after the Rh mirror. The beam was focused on the sample on a spot of  $0.6$  (vertical)  $\times$   $2$  mm (axial), with a flux of the order of  $10^{10}$  photons  $\text{mm}^{-2}$   $\text{s}^{-1}$ . The sample was mounted onto the Eulerian cradle of a Huber 6 + 2-circle diffractometer with a vertical scattering plane (sample surface normal direction in the horizontal plane) for the 220 in-plane reflection with a grazing incidence of 0.2 degrees. X-ray diffraction data were collected with a Pilatus 100 K area detector (pixel size of 172  $\mu\text{m}$ ). The sample-to-detector distance was set to 813 mm and air absorption was minimized using evacuated fly tubes. The axial intensity distribution (along the detector area width, horizontal direction) has been integrated when composing the two-dimensional reciprocal space maps.<sup>28,29</sup>

In-plane misorientation of the membranes, *i.e.*, their rotation around the growth direction, is given by  $\Delta\theta \approx \Delta Q_x/Q_{220}$ , while the in-plane lattice parameter is obtained from the maps referring to the GaAs lattice parameter where  $\Delta Q_z = Q_z - Q_{220}$  and  $Q_{220} = 2\pi/d_{220}$  with  $d_{220}$  being the atomic interplane distance of Bragg planes along the [220] in-plane direction. In other words, the scattering vector of the (220) in-plane GaAs reflection  $Q_{220}$  is taken as zero of the map.

Micro-Photoluminescence ( $\mu\text{-PL}$ ) measurements were performed using the setups of the optical spectroscopy group at the Physics Institute of the University of Campinas. Samples were excited using a 405 nm solid state laser line, with a power of 20  $\mu\text{W}$ , through a home-built microscope setup with a  $50\times$  long working distance objective lens (producing a *ca.* 2  $\mu\text{m}$  wide laser spot) and cooled in a cold-finger Cryovac He cryostat at 13 K. PL spectra were acquired using a 0.5 m Andor spectrometer equipped with a Si-CCD camera.

Transition energies and transition matrix elements of the QW structure were calculated using the latest version of nextnano software (Nextnano GmbH).<sup>30</sup> The InAlGaAs/InGaAs/InAlGaAs QW was modeled as a 1-dimensional line problem, and material parameters (like bandgap, strain induced shifts of the electronic structure, *etc.*) were provided by the material database of the program. QW well structure was implemented

using the nominal growth parameters and the optical transitions were calculated for a temperature of 10 K for a fully strained and unstrained QW. The input file was based on the provided nextnano tutorial for the optical transitions of an InGaAs QW with GaAs barriers.

## Results and discussion

Our approach to strain engineer III-V heterostructures is illustrated in Fig. 1(b)–(d). We grow an initial epitaxial layer system containing an AlAs sacrificial layer, which is lithographically patterned to form areas for releasing and in-place bonding as illustrated in Fig. 1(b). Virtual substrates are fabricated by the release of the top 5 nm GaAs/10 nm  $\text{In}_{0.2}\text{Ga}_{0.8}\text{As}$ /5 nm GaAs by selective removal of the sacrificial layer. As shown in previous studies,<sup>24</sup> after releasing the strained top the heterostructure will relax to its average lattice parameter – in our case the membrane has an average lattice parameter of 5.6938 Å, similar to a pure  $\text{In}_{0.1}\text{Ga}_{0.9}\text{As}$  bulk crystal. Due to geometrical restrictions, the released GaAs/InGaAs/GaAs layer forms a wrinkled network as illustrated in Fig. 1(c).<sup>24,31</sup> At this point, fabricated membranes can be transferred to a new host substrate as we demonstrate in the ESI.†

After the formation of the wrinkled, relaxed, in-place bonded membranes, the samples are chemically cleaned and reintroduced into the MBE. We deposited 10 nm thick  $\text{In}_x\text{Ga}_{1-x}\text{As}$  layers varying the indium content from  $x = 0.05$  to  $x = 1$ , which corresponds to the step illustrated in Fig. 1(d), and the distribution of the deposited material was analyzed *ex situ* after growth.

It is worth pointing out that during the complete release most of the membranes bond back to the substrate at the previously defined mesa position, as can be seen in Fig. 1(e), which shows a light microscopy image of three mesas with wrinkled membranes on top. But some tend to swim off in the wet chemical etching solution, leaving behind a bare GaAs (001) substrate as shown in the clean circle in Fig. 1(e). As the surface quality is like the one of the released membrane undergoing the same cleaning process, these areas are ideal references to compare the growth on top of the membrane with that on a ridged bulk GaAs surface. Finally, Fig. 1(f) depicts a magnified light microscopy image of a membrane used as a virtual substrate. The mesa has a diameter of 150  $\mu\text{m}$  and the wrinkled membrane on top of it is clearly identifiable. The light microscopy image demonstrates that there are large flat areas between the wrinkles, which could be maximized by a more advanced lift-off and membrane transfer process.<sup>32</sup>

In our systematic overgrowth study, RHEED indicated a change in the crystal growth mode from 2D to 3D for indium concentrations between 30% and 50%. Therefore, we carried out an overview examination by SEM of samples with 30%, 40% and 50% indium contents. The obtained images are shown in Fig. 2(a)–(f).

The larger scale image in Fig. 2(a) obtained from a surface with 10 nm  $\text{In}_{0.3}\text{Ga}_{0.7}\text{As}$  demonstrates that the wrinkled mem-

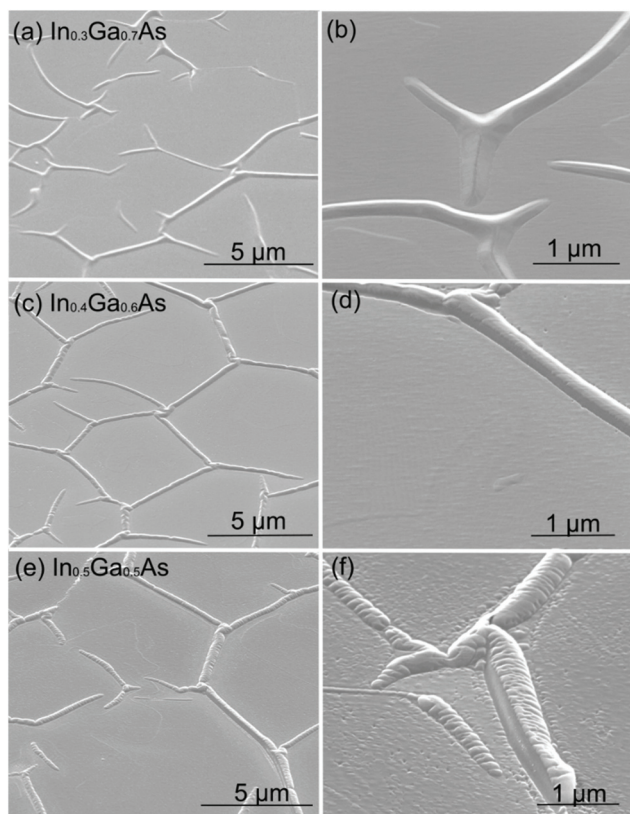


**Fig. 2** (a)–(f) Overview of the SEM images of overgrown membranes with 10 nm of InGaAs with different In-contents. The SEM demonstrates that the membranes stay intact during overgrowth. (a)–(b) 10 nm  $\text{In}_{0.3}\text{Ga}_{0.7}\text{As}$ , (c)–(d) 10 nm  $\text{In}_{0.4}\text{Ga}_{0.6}\text{As}$ , and (e)–(f) 10 nm  $\text{In}_{0.5}\text{Ga}_{0.5}\text{As}$ . With the increase of In-content, we observe an increase in the roughness of the surface as well as material accumulation on top of the wrinkles.

brane stays intact during the whole growth procedure, similarly to the 40% sample shown in Fig. 2(c). Furthermore, there is no indication of surface roughening or accumulation of material on top of wrinkles as we observed for partly released membranes overgrown with pure InAs.<sup>11</sup> Indeed, the magnified SEM image of Fig. 2(b) indicates a slight depletion of material on top of the wrinkle. Away from the wrinkle a flat film growth is observed. Comparing Fig. 2(b) and (d), we observe a change in the wrinkle covering and a slight roughening of the surface, but no formation of island structures or a clear material accumulation. It now appears that the wrinkled side walls are less covered (see Fig. 2(d)) and the material prefers to stay on top of the wrinkles. Such behavior indicates a change in material–membrane–strain interaction, rendering parts of the sample less attractive for material deposition.<sup>10,11</sup> Finally, reaching an indium concentration of 50%, we see a clear change in the overgrowth behavior. The surfaces in Fig. 2(e) and (f) appear to be rough and we observe material accumulation on the wrinkles.

To study the change from a 2D growth mode to a 3D one in more detail,  $2 \times 2 \mu\text{m}^2$  sized AFM topography images of

the membrane as well as a GaAs reference surface on each sample are obtained as depicted in Fig. 3. To accomplish a complete study, samples with 10 nm  $\text{In}_x\text{Ga}_{x-1}\text{As}$  are depicted by varying  $x = 0$  (as processed), 0.05, 0.3, 0.4, 0.5, to pure InAs ( $x = 1$ ).

The AFM investigation of the initial surface (Fig. 3(a) and (g)) demonstrates that both the membrane (Fig. 3(a)) and the areas of the sample exhibiting a relaxed GaAs (001) surface (Fig. 3(g)) are flat and clean. For the deposition of low indium content alloys like  $x = 0.05, 0.1, \text{ and } 0.2$ , we always observe good layer-by-layer growth with the typical 2D islands for a flat material, both for the membrane and for the bare GaAs surface. As an example of these surfaces, we depict the  $\text{In}_{0.05}\text{Ga}_{0.95}\text{As}$  surface in Fig. 3(b) and (h) –  $\text{In}_{0.1}\text{Ga}_{0.9}\text{As}$  and  $\text{In}_{0.2}\text{Ga}_{0.8}\text{As}$  surfaces are depicted in the ESI.† Reaching higher indium content, we would expect to change the growth mode from a Franck–van der Merwe growth mode to a Stranski–Krastanov one with the formation of 3D islands. Depending on the exact growth conditions, this transition should occur – in our experience – between 30% and 40% of indium content with a critical thickness of less than 10 nm (the film thickness grown in our samples).<sup>33,34</sup> Indeed, we still observe a flat layer growth for both the membrane and the GaAs surface as seen in Fig. 3(c) and (i), as expected from the SEM images depicted in Fig. 2(a) and (b). Compared to the membrane, the 2D islands on the bare GaAs appear to be slightly larger, but both surfaces exhibit the same roughness. For the bare GaAs surface, we recognize the presence of carbon pits ascribed to a local failing of the cleaning process of the sample.

Interestingly, the surface of the 40% InGaAs alloy on the membrane and the GaAs surface appear to be different. As expected from the SEM images, the surface on the membrane is slightly rougher compared to the surface of the lower indium content alloys, and we observe the onset of island formation (Fig. 3d). The AFM image in Fig. 3(j) of the InGaAs film deposited on the GaAs surface demonstrates that the InGaAs has been grown beyond the critical thickness of the material, which is expected to be 1–2 nm for an  $\text{In}_{0.4}\text{Ga}_{0.6}\text{As}$  film.<sup>16,33</sup> Hence, the critical thickness on top of the membrane is significantly larger than the one on bare GaAs. This occurs because the membrane relaxes to its average net lattice parameter. The misfit strain of the deposited  $\text{In}_{0.4}\text{Ga}_{0.6}\text{As}$  layer decreases from  $-2.86\%$  (on GaAs) to  $-2.13\%$  on the membrane – a value comparable to the misfit of  $\text{In}_{0.3}\text{Ga}_{0.7}\text{As}$  on GaAs, where we observe a flat layer growth.<sup>16,33</sup>

As indicated by the RHEED and by the SEM investigation depicted in Fig. 2, we expected a breakdown of the layer-by-layer growth mode for InGaAs alloys at indium contents larger than 50%. Indeed, we see the formation of islands and an extreme roughening of the surface in the AFM images for the 10 nm  $\text{In}_{0.5}\text{Ga}_{0.5}\text{As}$  and InAs film on the membrane and on the pure GaAs (Fig. 3(e), (k), (f) and (l), respectively). It is worth pointing out that growth on the membrane seems to be significantly different from the bare GaAs surface. In AFM, we observe the formation of bubbles on the membrane (Fig. 3(e))

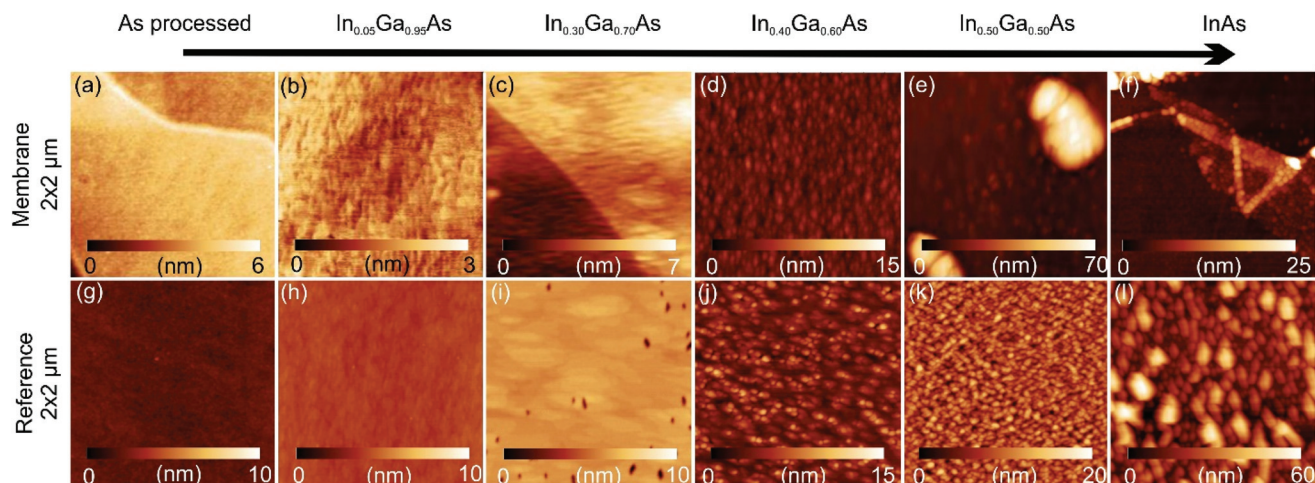


**Fig. 3** AFM study of the overgrowth effect. Column-wise, we depict different In concentrations ranging from an initial surface, without an alloy, to pure InAs deposition always comparing the overgrown membrane surface to the bare GaAs surface on the same sample (lower column). At an In concentration of 40%, growth on the bare GaAs breaks down (dot and misfit dislocation formation), whereas the material on the membrane stays significantly flatter and appears to be still coherent. At 50%, we observe the formation of bubbles on the membrane (image (e)) and material accumulation on top of the bubbles. Pure InAs forms large islands on the bare GaAs but accumulates on top of the membranes, forming large islands surrounded by relatively material free areas.

as well as preferred material migration and accumulation (Fig. 3(e) and (f)), whereas the material deposited on the GaAs surface only exhibits larger dots (Fig. 3(k) and (l)). The formation of bubbles is ascribed to a transfer of the misfit strain from the deposited material to a thin compliant substrate.<sup>9</sup> Material migration to the top of the wrinkles and accumulation on certain positions arise from the modulation of the surface energy and misfit strain due to membrane curvature and some strain transfer to the compliant substrate.<sup>10,11</sup> For highly strained materials like  $\text{In}_{0.7}\text{Ga}_{0.3}\text{As}$  and pure InAs, the formation of large material clusters on top of the membrane is observed (see Fig. 3(f) and the ESI†). It is also worth mentioning that the membrane always seems to be preferred by the deposited strained material as we observe migration of material from the bare GaAs surface towards the membrane (see the ESI†).

To demonstrate coherent growth and strain transfer to the in-place bonded membrane, we carried out grazing incidence X-ray diffraction to analyze the lattice parameter distribution inside our samples. As the XRD spot under grazing incidence covers a large area on the sample, we obtain average strain information of the whole sample compared to more local methods like SEM and AFM. Two-dimensional reciprocal space maps (RSMs) around the in-plane (220) GaAs reflection are shown in Fig. 4. The main features related to the membrane overgrown process are diffuse intensity distributions in the lower portion of the maps where  $\Delta Q_z < 0$ , evidencing structures with an in-plane lattice parameter larger than the substrate one. Diffractions from fully strained structures to the substrate lattice are only distinguished from the GaAs peak when possessing slight in-plane misalignments where  $\Delta Q_x \neq 0$ , as seen for instance in Fig. 4(a), (d), and (e). The intensity of the substrate peak is very susceptible to the

grazing angle when above the critical angle, which is 0.31 degrees for a flat GaAs surface. In patterned surfaces, this critical angle can be smaller, which explains the observed variation in the substrate peak intensity from one map to another, such as seen from Fig. 4(a) to 4(b) and (c), due to an inaccuracy of about 0.1 degrees in aligning the grazing angle of each sample.

The RSM of the as-processed membrane is depicted in Fig. 4(a). We observe an intense diffraction at the GaAs position and a diffuse weaker intensity with a maximum at  $\Delta Q_z = -2.5$  r.l.u. This  $\Delta Q_z$  value agrees well with the expected position of  $\Delta Q_z = -2.23$  r.l.u. for the completely relaxed membrane. In the RSMs of the other post-grown samples, a broad diffuse (red color) feature appears below the GaAs position. It corresponds to the signal from the membrane with the material deposited (membrane + layer), which shifts down systematically as the indium content increases. The RSMs of the samples with 5% (Fig. 4(b)) and 30% (Fig. 4(c)) indium content confirm our assumption that they are coherent to the membranes since  $\Delta Q_z = -1.9$  r.l.u. and  $\Delta Q_z = -3.7$  r.l.u. are, respectively, the expected positions for relaxed structures with the membrane + layer average compositions (average lattice parameter of 5 nm GaAs/10  $\text{In}_{0.2}\text{Ga}_{0.8}\text{As}$ /5 nm GaAs membrane plus a 10 nm layer of overgrown  $\text{In}_x\text{Ga}_{1-x}\text{As}$ , as indicated in the maps by dashed lines with the tag “membrane + layer”). Note that no intensity towards the predicted position (dashed line with the tag “bulk”) for a relaxed  $\text{In}_{0.3}\text{Ga}_{0.7}\text{As}$  compound is visible in Fig. 4(c).

Remarkably, a drastic change in the coherence of the overgrown layer is seen when analyzing the RSMs in Fig. 4(d) and (e) of samples with higher indium content. For the 40% film, Fig. 4(d) shows similar behavior to the previous films of lower indium content where the red diffuse contributions are close

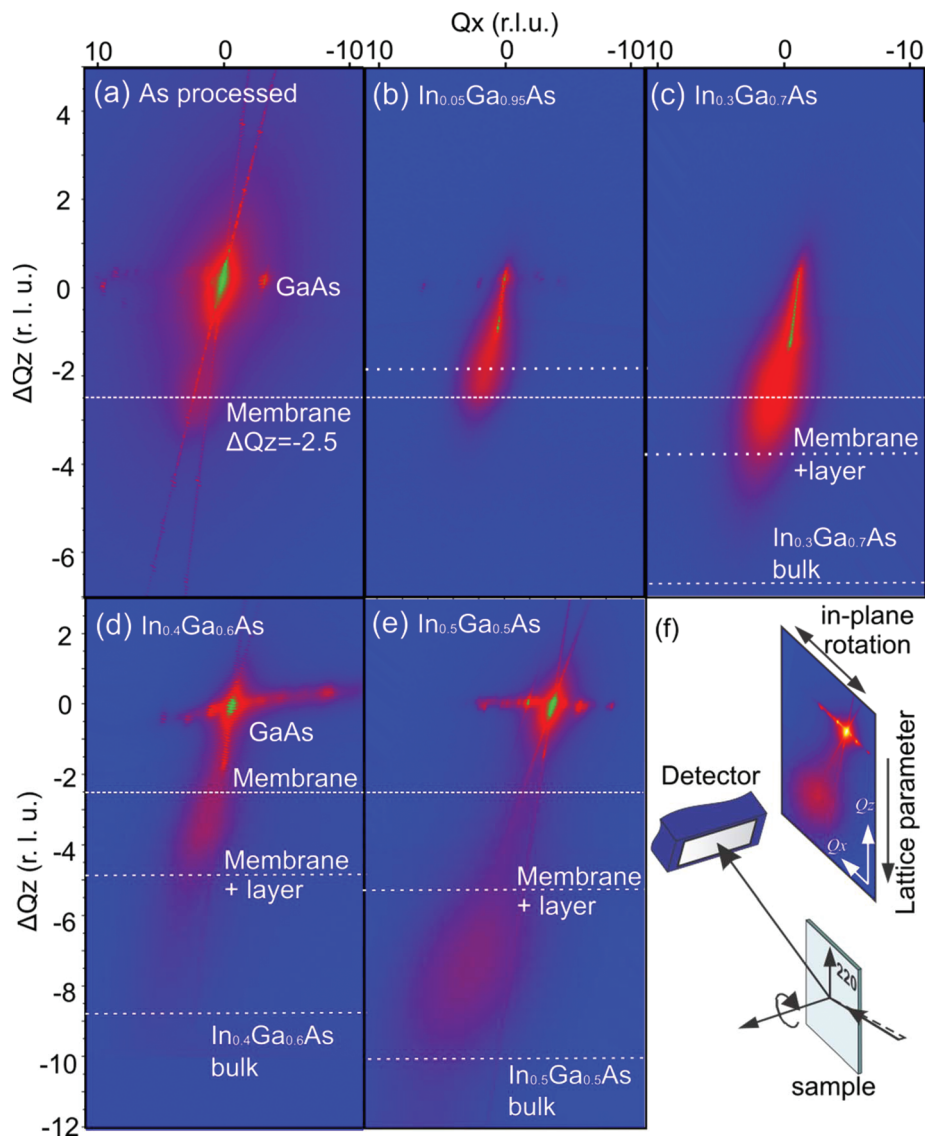


**Fig. 4** (a)–(e) XRD reciprocal space maps (RSMs) of samples with varying In contents. Panel (f) illustrates the diffraction geometry and the information of the maps, where  $1 \text{ r.l.u.} = 0.01 \text{ \AA}^{-1}$ . Up to 30% In content, we observe straining of the membrane and epitaxial growth behavior. From 40% indium content a tail to larger lattice parameters is observed, indicating the onset of relaxation. Finally, a clear satellite structure is observed for 50% (or higher) indium content, indicating the breakdown of epitaxy.

to the parameter of the relaxed membrane. However, in this sample it is more evident that the diffuse feature is at an intermediate value between the membrane and relaxed membrane + layer net parameters. The latter indicates that the  $\text{In}_{0.4}\text{Ga}_{0.6}\text{As}$  transfers partially some of its strain to the membrane, shifting the film/membrane heterostructure to a large lattice parameter. Hence, the membrane acts like a compliant substrate, but it is still slightly bonded to the underlying GaAs and not completely flexible. Therefore, most of the deposited  $\text{In}_{0.4}\text{Ga}_{0.6}\text{As}$  is compressed to a lattice parameter between the membrane and the film/membrane lattice parameters. From the shape and the position of the in-plane film/membrane XRD, we can assume that the deposited material is mostly coherent towards the underlying virtual substrate formed by

the membrane – an assumption that is well supported by the SEM and AFM results. An intensity tail indicates partial relaxation of the deposited material towards higher lattice parameters, *e.g.*, due to the formation of incoherent islands or dislocations which can occur on the area of the bare GaAs.

However, for the 50% film deposited on the membrane, Fig. 4(e) shows very different behavior where the diffuse contribution lies after the membrane + layer parameter line, *i.e.*, in between the membrane + layer parameter and the parameter of a completely relaxed InGaAs layer. Hence, the deposited material is most likely not coherent towards the membrane anymore, but still partly strained. The broadening in the  $Q_x$  direction further supports the loss of coherence, as we would expect from the SEM and AFM images. The material accumu-

lation most likely leads to a loss of the epitaxial film/substrate relationship. We would like to point out that no clear separation of membrane and deposited film peaks are observed, indicating that the membrane is indeed counter strained by the  $\text{In}_{0.5}\text{Ga}_{0.5}\text{As}$  layer. We speculate that this is due to the formation of the bubbles observed in the AFM topography analysis (Fig. 3(e)).

So far, only the structural properties of the relaxed in-place bonded membranes and the deposited films have been discussed. However, for using them as virtual substrates, it is necessary to demonstrate the ability to grow optical and/or electrical functional structures on top of them and to understand the effects of the different strain states of the virtual substrate on the optical/electrical properties of these structures.

Fig. 5 depicts the surface and the low temperature  $\mu$ -PL spectra of  $\text{In}_{0.10}\text{Al}_{0.20}\text{Ga}_{0.70}\text{As}/\text{In}_{0.10}\text{Ga}_{0.90}\text{As}/\text{In}_{0.10}\text{Al}_{0.20}\text{Ga}_{0.70}\text{As}$  QWs grown on a GaAs (001) substrate (reference sample) and on a partly released, in-place bonded GaAs/InGaAs/GaAs membrane used in the previous experiments. Fig. 5(a) depicts an AFM topography image of the grown structure on top of the membrane, demonstrating that we obtained a flat,

layer-by-layer growth mode for the whole structure. The optically active structure is illustrated in the inset of Fig. 5(b) – in both cases the QW structure was capped with a 5 nm  $\text{In}_{0.10}\text{Ga}_{0.90}\text{As}$  layer for surface protection.

The image plot of PL spectra in the inset of Fig. 5(c) corresponds to a linear scan along the membrane surface with 0.5  $\mu\text{m}$  steps. Typical spectra from membrane and reference samples are shown in the main plot of Fig. 5(c). Here, the spectra have been taken under the same conditions to allow a comparison of the intensities. The reference sample has a single emission peak at 1.48 eV (836.5 nm) with a line width of 0.7 meV (3.1 nm). This position is in very good agreement with the calculated position for such a structure by nextnano (1.49 eV) for the electron-heavy hole transition in a strained  $\text{In}_{0.10}\text{Al}_{0.20}\text{Ga}_{0.70}\text{As}/\text{In}_{0.10}\text{Ga}_{0.90}\text{As}/\text{In}_{0.10}\text{Al}_{0.20}\text{Ga}_{0.70}\text{As}$  QW on GaAs. The signal strength from the QW grown on the membrane is on average 0.1 to 0.2 times the signal strength of the reference sample, broader (1.45 meV) and red shifted (*ca.* 30 meV). The peak is at 1.458 eV for the spectrum shown in Fig. 5, and around 1.45 eV for the spectra shown in the inset. The image plot shows that it is homogeneous over the sample, but at some positions shifted still to the position of the reference sample.

Using a complete relaxed structure, we expect the peak at 1.45 eV from nextnano calculations. The observed redshift between 30 and 40 meV is in good agreement with the previously given estimation (40 meV) as well as with the calculation done using the k-p theory (35 meV by nextnano). At some positions, the image plot (inset of Fig. 5(c)) shows the appearance of more than one peak, besides the fact that only a single peak is observed in most cases. The fluctuation of the peak position is ascribed to the fluctuation of the QW size and the indium content of the ternary alloy on top of the membrane. As these fluctuations likely arise from the modification of the chemical surface potential due to the wrinkling of the membrane, we expect them to vanish if wrinkling is suppressed or avoided by more advanced preparation methods, *e.g.* lift-off by floating demonstrated in the past.<sup>2,3,32</sup> As we have some control over the wrinkling process,<sup>35–37</sup> they can also be used to further strain engineer the quantum well emission.

We want to point out that, besides being weaker than the reference sample, PL detection from the QW on the membrane is a remarkable achievement, given all the chemical processes prior to post-growth. Surprisingly, we are also able to observe the PL signal from the membrane at room temperature (see ESI Fig. 4†). Even though the barriers are very thin, the material quality on top of the membrane is already high enough to allow functioning under device relevant conditions (ambient temperature). As the QW is only separated by the membrane surface, which has undergone processing and cleaning, by a 20 nm  $\text{In}_{0.10}\text{Ga}_{0.90}\text{As}$  spacer layer, we attribute the intensity reduction of the optical signal to surface state effects. This is a well-known problem for structures grown on patterned substrates<sup>38</sup> and could be resolved by thicker spacer layers between the virtual membrane and the active structure.

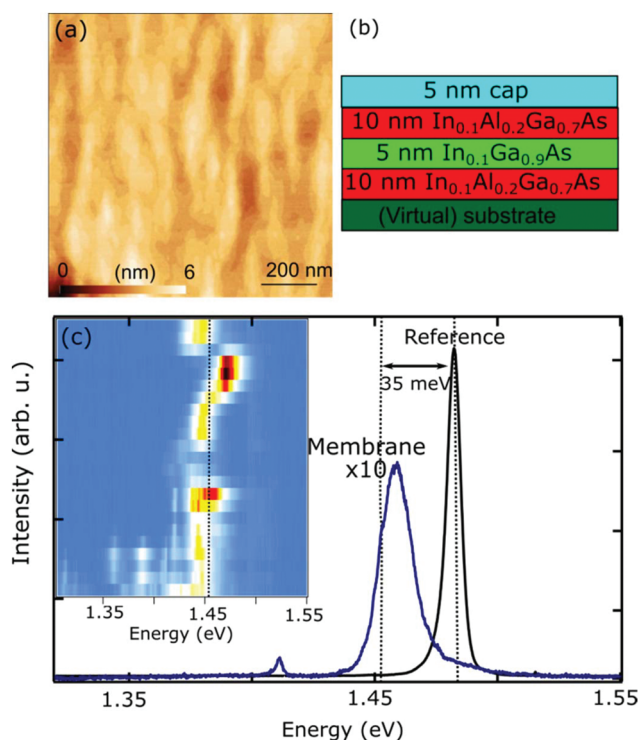


**Fig. 5** (a) AFM image of the surface demonstrating good 2D growth on top of the membrane. (b) The schematic diagram depicts the grown structure of the QW on the membrane and on the GaAs (001) substrate. (c)  $\mu$ -PL spectra from an InAlGaAs/InGaAs/InAlGaAs QW grown on a membrane (black spectrum) and on a GaAs (001) substrate (blue line). The inset depicts  $\mu$ -PL spectra corresponding to a linear spatial scan on the membrane with 0.5  $\mu\text{m}$  steps. We note a good luminescence signal from the QW on the membrane even though it is grown close to the processed interface. These spectra exhibit a red shift indicating that it is less strained than the QW on the GaAs (001) substrate as expected for the relaxed membrane.

## Conclusion

Our systematic overgrowth study of relaxed in-place bonded GaAs/InGaAs/GaAs membranes shows that they can serve as compliant substrates for III-V heteroepitaxy. We demonstrate the ability to grow flat layers as well as observe an increase in the critical thickness for dot formation. SEM and AFM images indicate a strain transfer and therefore a changed growth behavior of the deposited material on the compliant substrate. XRD investigations show that the deposited films stay coherent beyond the critical thickness of InGaAs deposited on bulk GaAs crystals as well as support the assumption of strain transfer from the deposited material to the membrane used as a virtual substrate. We also demonstrate the ability to grow good quality optical active structures on top of the membranes. The PL results confirm our assumption that the membrane used as a virtual substrate allows for the growth of an unstrained InGaAs heterostructure. Taking into account that this kind of membranes are transferable to any substrates before growth like InP or Si,<sup>3,22,24,32</sup> this work opens the door to an alternative strain engineering of heterostructures on any substrate of choice.<sup>14,15,39</sup> Furthermore, as a thin membrane (we previously demonstrated lift-off of InAs/GaAs layers as thin as  $\approx 1$  nm (ref. 8)) is used as the substrate, one can tune the lattice parameter of the membrane in the entire range of the InGaAs alloys and then grow the desired unstrained heterostructure on an arbitrary substrate, hence overcoming the restriction of the reverse process of first growing, then releasing, and transferring the heterostructure.

## Conflicts of interest

There are no conflicts of interest.

## Acknowledgements

C. D. acknowledges financial support from the FAPESP (2016/14001-7) and the CNPq (423962/2016-7), O. C. from FAPESP (2012/11 382-9), and F. I. from FAPESP (2016/16365) and CNPq (305769/2015-4). Beamtime was granted by the LNLS on XRD2 and we want to thank the beamline staff for their technical support. We acknowledge the access to the SEM of the LME group of the LNNano/CNPEM. S. F. C. and S. L. M. acknowledge financial support from the Coordenação de Aperfeiçoamento de Pessoal de Nível Superior – Brasil (CAPES). We thank for access to the clean room of the LMF and DSF of the LNNano.

## References

- 1 V. Y. Prinz, V. A. Seleznev, A. K. Gutakovskiy, A. V. Chehovskiy, V. V. Preobrazhenskii, M. A. Putyato and T. A. Gavrilova, *Phys. E*, 2000, **6**, 828–831.
- 2 M. G. Lagally, *MRS Bull.*, 2007, **32**, 57–63.
- 3 J. A. Rogers, M. G. Lagally and R. G. Nuzzo, *Nature*, 2011, **477**, 45–53.
- 4 J. A. Rogers and J.-H. Ahn, *Silicon Nanomembranes: Fundamental Science and Applications*, Wiley, 2016.
- 5 O. G. Schmidt, C. Deneke, Y. Nakamura, R. Zapf-Gottwick, C. Muller and N. Y. Jin-Phillipp, *Adv. Solid State Phys.*, 2002, **42**, 231–240.
- 6 O. G. Schmidt, N. Schmarje, C. Deneke, C. Muller and N. Y. Jin-Phillipp, *Adv. Mater.*, 2001, **13**, 756–759.
- 7 M. H. Huang, P. Rugheimer, M. G. Lagally and F. Liu, *Phys. Rev. B: Condens. Matter Mater. Phys.*, 2005, **72**, 085450.
- 8 C. Deneke, A. Malachias, S. Kiravittaya, M. Benyoucef, T. H. Metzger and O. G. Schmidt, *Appl. Phys. Lett.*, 2010, **96**, 143101.
- 9 C. Deneke, A. Malachias, A. Rastelli, L. Mercus, M. Huang, F. Cavallo, O. G. Schmidt and M. G. Lagally, *ACS Nano*, 2012, **6**, 10287–10295.
- 10 S. F. C. da Silva, E. M. Lanzoni, V. de A. Barboza, A. Malachias, S. Kiravittaya and C. Deneke, *Nanotechnology*, 2014, **25**, 455603.
- 11 S. F. C. da Silva, E. M. Lanzoni, A. Malachias and C. Deneke, *J. Cryst. Growth*, 2015, **425**, 39–42.
- 12 C. S. Ritz, H. J. Kim-Lee, D. M. Detert, M. M. Kelly, F. S. Flack, D. E. Savage, Z. Cai, P. G. Evans, K. T. Turner and M. G. Lagally, *New J. Phys.*, 2010, **12**, 103011.
- 13 H. J. Kim-Lee, D. E. Savage, C. S. Ritz, M. G. Lagally and K. T. Turner, *Phys. Rev. Lett.*, 2009, **102**, 226103.
- 14 S. A. Scott, C. Deneke, D. M. Paskiewicz, H. J. Ryu, A. Malachias, S. Baunack, O. G. Schmidt, D. E. Savage, M. A. Eriksson and M. G. Lagally, *ACS Appl. Mater. Interfaces*, 2017, **9**, 42372–42382.
- 15 P. Sookchoo, F. F. Sudradjat, A. M. Kiefer, H. Durmaz, R. Paiella and M. G. Lagally, *ACS Nano*, 2013, **7**, 2326–2334.
- 16 H. Morkoc, B. Sverdlov and G.-B. Gao, *Proc. IEEE*, 1993, **81**, 493–556.
- 17 J. E. Ayers, *J. Electron. Mater.*, 2008, **37**, 1511–1523.
- 18 F. H. Pollak, in *Strained layer superlattices: Physics*, Academic Press, vol. 32, p. 17.
- 19 Y. H. Lo, *Appl. Phys. Lett.*, 1991, **59**, 2311.
- 20 F. E. Ejeckam, Y. H. Lo, S. Subramanian, H. Q. Hou and B. E. Hammons, *Appl. Phys. Lett.*, 1997, **70**, 1685.
- 21 A. M. Jones, J. L. Jewell, J. C. Mabon, E. E. Reuter, S. G. Bishop, S. D. Roh and J. J. Coleman, *Appl. Phys. Lett.*, 1999, **74**, 1000.
- 22 F. Cavallo and M. G. Lagally, *Soft Matter*, 2010, **6**, 439–455.
- 23 D. L. Owen, D. Lackner, O. J. Pitts, S. P. Watkins and P. M. Mooney, *Semicond. Sci. Technol.*, 2009, **24**, 035011.
- 24 A. Malachias, Y. F. Mei, R. K. Annabattula, C. Deneke, P. R. Onck and O. G. Schmidt, *ACS Nano*, 2008, **2**, 1715–1721.
- 25 M. Zamiri, F. Anwar, B. A. Klein, A. Rasoulof, N. M. Dawson, T. Schuler-Sandy, C. F. Deneke, S. O. Ferreira, F. Cavallo and S. Krishna, *Proc. Natl. Acad. Sci. U. S. A.*, 2017, **114**, E1–E8.
- 26 J. A. Rogers, *ACS Nano*, 2007, **1**, 151–153.



- 27 X. Wang, X. Cui, A. Bhat, D. E. Savage, J. L. Reno, M. G. Lagally and R. Paiella, *Appl. Phys. Lett.*, 2018, **113**, 201105.
- 28 S. L. Morelhão, *Computer Simulation Tools for X-ray Analysis*, Springer International Publishing, Cham, 2016.
- 29 S. L. Morelhão, C. I. Fornari, P. H. O. Rappl and E. Abramof, *J. Appl. Crystallogr.*, 2017, **50**, 399–410.
- 30 *nextnano – Software for semiconductor nanodevices*, <https://www.nextnano.de/> (accessed July 12, 2018).
- 31 Y. F. Mei, S. Kiravittaya, M. Benyoucef, D. J. Thurmer, T. Zander, C. Deneke, F. Cavallo, A. Rastelli and O. G. Schmidt, *Nano Lett.*, 2007, **7**, 1676–1679.
- 32 C.-W. Cheng, K.-T. Shiu, N. Li, S.-J. Han, L. Shi and D. K. Sadana, *Nat. Commun.*, 2013, **4**, 1577.
- 33 M. Pristovsek, R. Kremzow and M. Kneissl, *Jpn. J. Appl. Phys.*, 2013, **52**, 041201.
- 34 S. Jha, X. Song, S. E. Babcock, T. F. Kuech, D. Wheeler, B. Wu, P. Fay and A. Seabaugh, *J. Cryst. Growth*, 2008, **310**, 4772–4775.
- 35 P. Cendula, S. Kiravittaya and O. G. Schmidt, *J. Appl. Phys.*, 2012, **111**, 043105.
- 36 P. Cendula, S. Kiravittaya, Y. F. Mei, C. Deneke and O. G. Schmidt, *Phys. Rev. B: Condens. Matter Mater. Phys.*, 2009, **79**, 085429.
- 37 Y. F. Mei, D. J. Thurmer, F. Cavallo, S. Kiravittaya and O. G. Schmidt, *Adv. Mater.*, 2007, **19**, 2124.
- 38 S. Kiravittaya, A. Rastelli and O. G. Schmidt, *Rep. Prog. Phys.*, 2009, **72**, 046502.
- 39 C. Deneke and S. F. Covre da Silva, *PCT/BR 2015/050157*, 2015.